

Supporting Information

Rational route to SCM materials based on 1-D cobalt selenocyanato coordination polymer

Jan Boeckmann and Christian Näther*

Figure Content	Page
S1 Thermal ellipsoid plot for 1 .	2
Tab.1 Selected bond lengths [Å] and angles [°] for 2 .	2
S2 DTG, TG, DTA and MS trend scan curves for 1 .	3
S3 Heating rate dependent TG measurements for 1 .	3
S4 Experimental XRPD patterns of the intermediates isolated in several TG runs.	4
S5 Isothermal XRPD measurements at 100°C of $[\text{Co}(\text{NCSe})_2(\text{pyridine})_4]$ (1).	4
S6 IR and Raman spectra for compound 1 .	5
S7 IR and Raman spectra for compound 2 .	5
S8 DC susceptibility measurements for $[\text{Co}(\text{NCSe})_2(\text{pyridine})_4]$ (1).	6
S9 Magnetization saturation experiments for $[\text{Co}(\text{NCSe})_2(\text{pyridine})_2]_n$ (2)	6
S10 Zero-field-cooled (ZFC) and field-cooled (FC) magnetic measurements for 2 .	7
S11 Isothermal frequency dependence of χ_M' and χ_M'' at 4.5 K for compound 2 .	7
S12 Plot of $\ln(\chi_M^* T)$ vs. T^1 for 2 .	8
S13 Experimental and calculated XRPD pattern for 1 .	8
S14 Difference plot of the Rietveld refinement of $[\text{Co}(\text{NCSe})_2(\text{pyridine})_2]_n$ (2).	9
S15 Experimental and calculated XRPD pattern for 2 .	9
- Further experimental details	10 ff

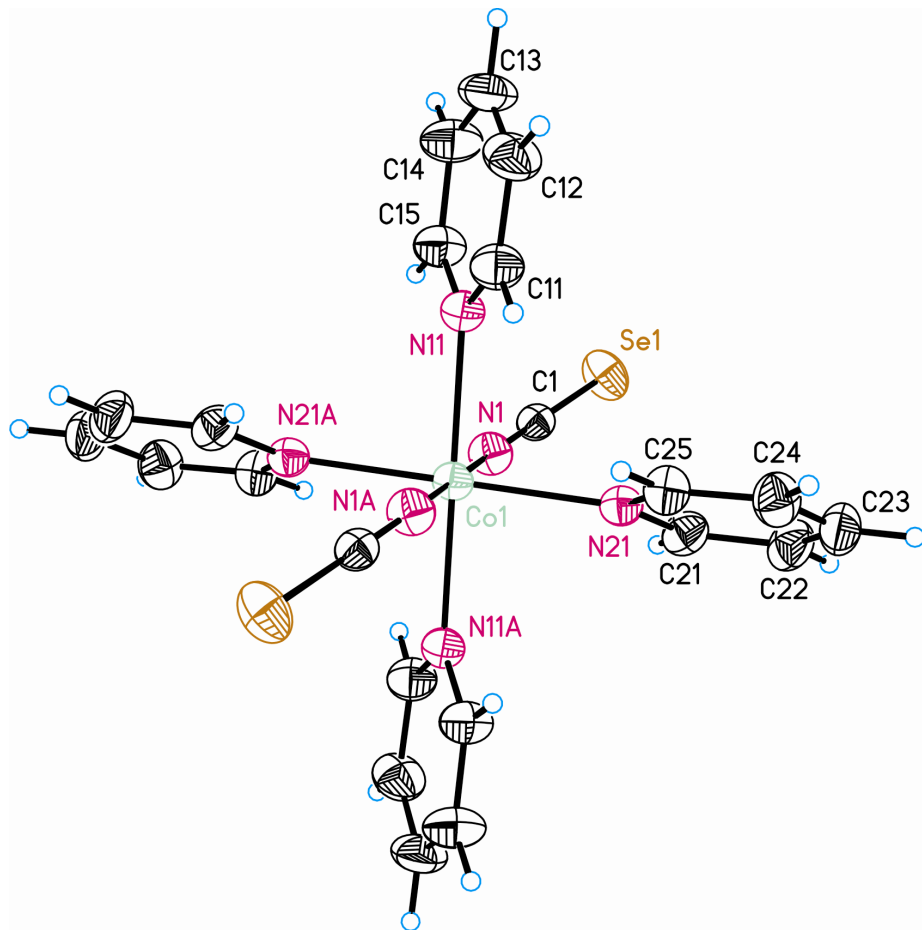


Figure S1. Thermal ellipsoid plot of the crystal structure of $[\text{Co}(\text{NCSe})_2(\text{pyridine})_4]$ (**1**) with view of the coordination sphere of the metal cation with labeling and displacement ellipsoids drawn at the 30% probability level. Symmetry codes: A = $-\text{x} + 3/2$, $-\text{y} + 3/2$, $-\text{z} + 1$.

Table 1. Selected bond lengths [\AA] and angles [$^\circ$] for **2**.

$[\text{Co}(\text{NCSe})_2(\text{pyridine})_2]_n$ (2)			
Co(1)-N(1A)	2.045(3)	Co(2)-N(31)	2.205(2)
Co(1)-N(2)	2.346(3)	Co(2)-Se(2)	2.5350(4)
Co(1)-N(11)	2.230(3)	N(1)-C(1)-Se(1)	176.2(2)
Co(1)-N(21)	2.266(3)	N(2)-C(2)-Se(2)	178.8(2)
Co(1)-Se(3)	2.7921(5)	N(3)-C(3)-Se(3)	178.8(3)
Co(1)-Se(1)	2.921(3)	N(11)-Co(1)-N(21)	174.63(11)
Co(2)-N(3)	2.193(3)	N(31)-Co(2)-N(31A)	180.0

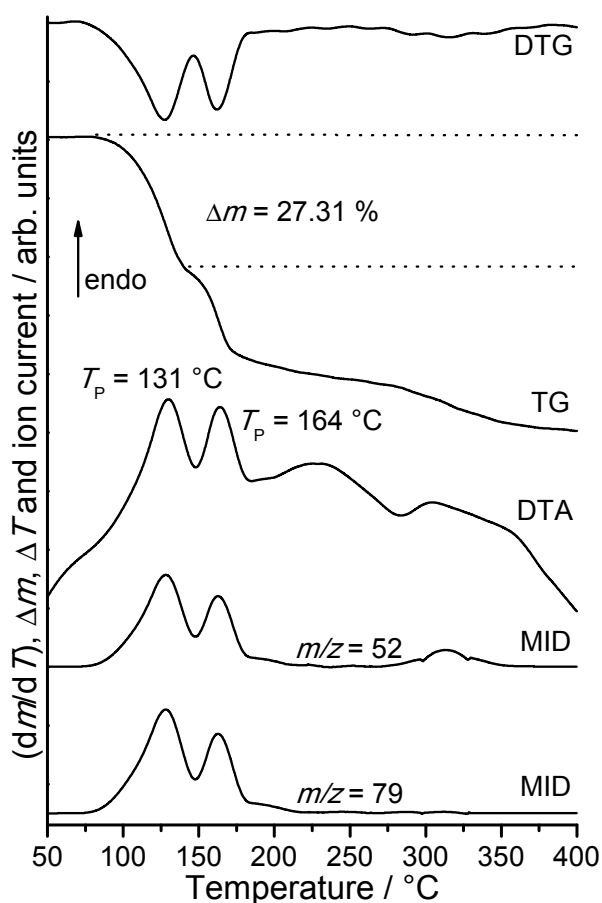


Figure S2. DTG, TG, DTA and MS trend scan curves of $[\text{Co}(\text{NCSe})_2(\text{pyridine})_4]$ (**1**). Heating rate = $4\text{ }^\circ\text{C}/\text{min}$; given are the peak temperatures T_p ($^\circ\text{C}$) and mass changes (%).

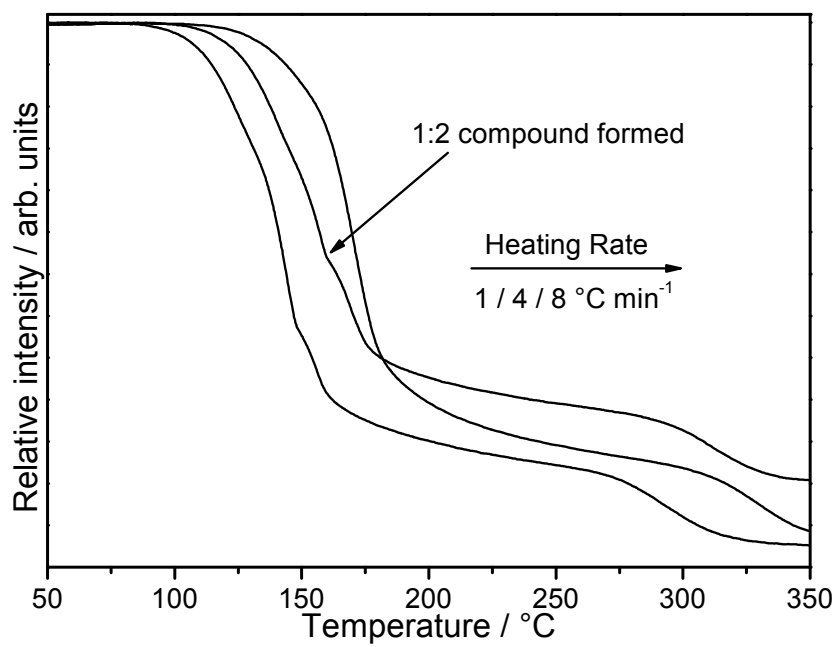


Figure S3. Heating rate dependent TG measurements for $[\text{Co}(\text{NCSe})_2(\text{pyridine})_4]$ (**1**).

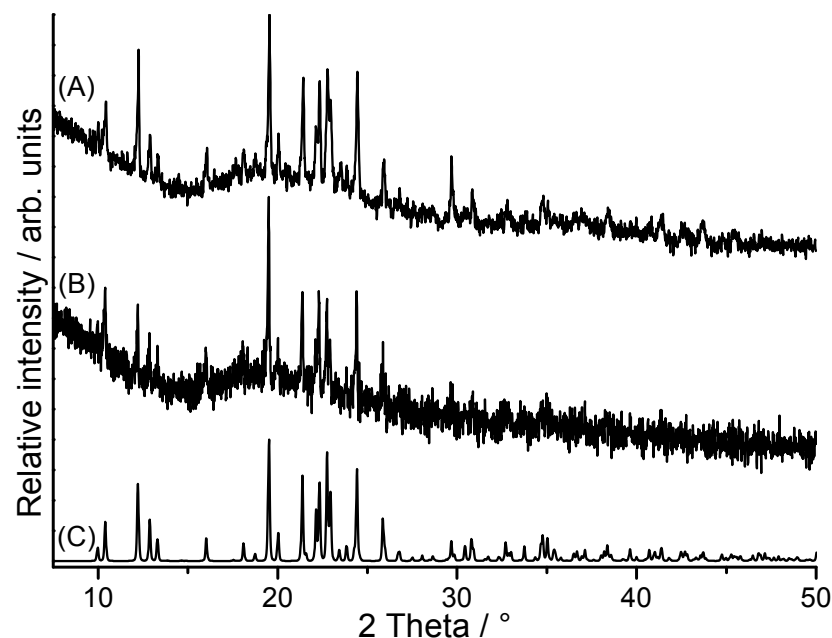


Figure S4. Experimental XRPD patterns of the intermediates isolated in several TG runs at about 160°C (A and B) together with calculated XRPD pattern (C) of $[\text{Co}(\text{NCSe})_2(\text{pyridine})_4]$ (**1**).

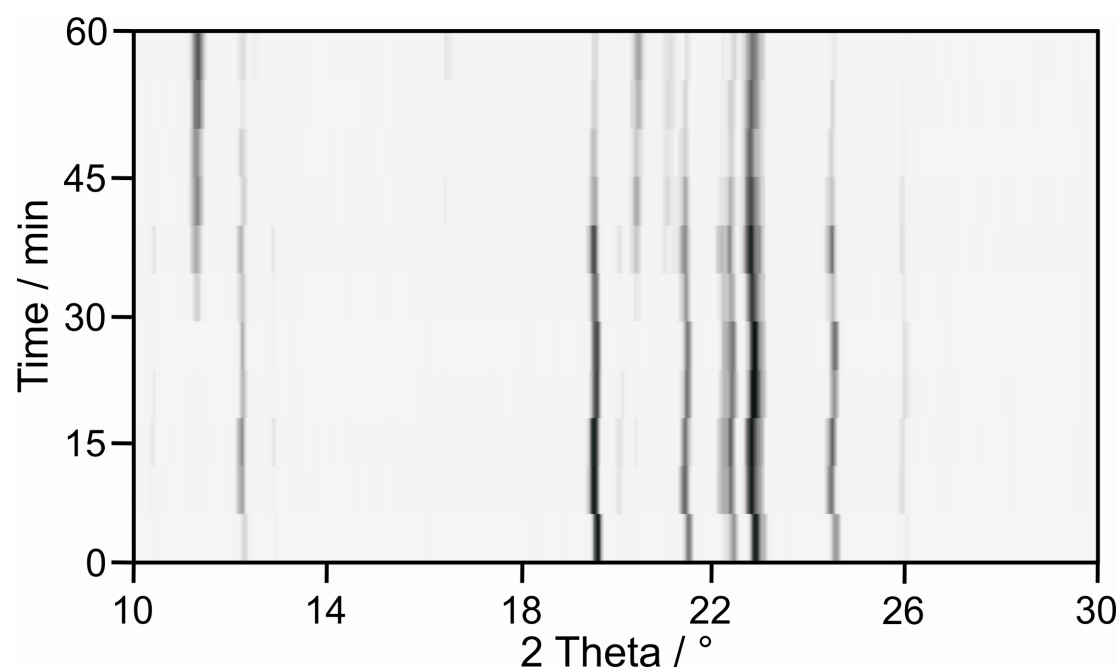


Figure S5. Isothermal XRPD measurements at 100°C of $[\text{Co}(\text{NCSe})_2(\text{pyridine})_4]$ (**1**).

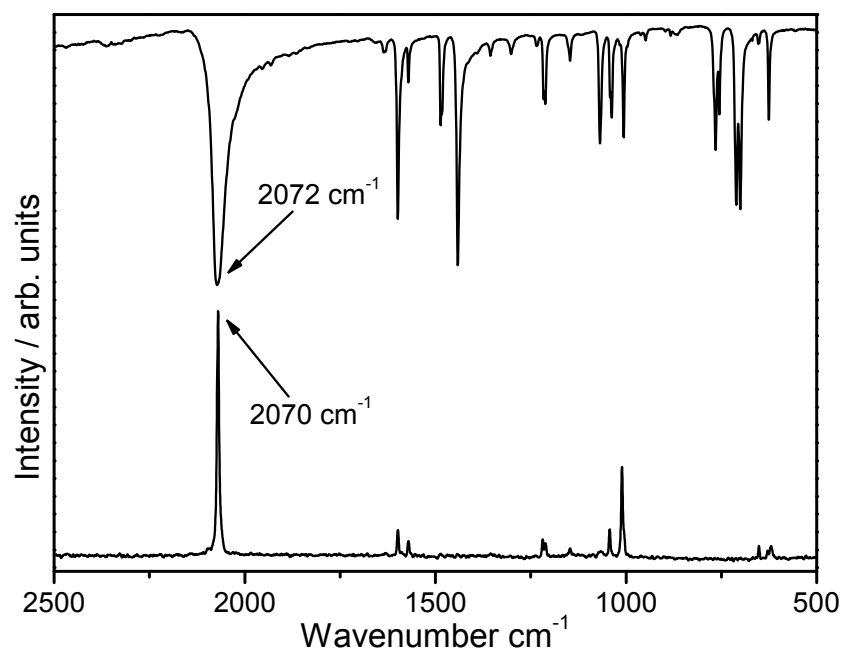


Figure S6. IR (top) and Raman (bottom) spectra for compound $[\text{Co}(\text{NCSe})_2(\text{pyridine})_4]$ (**1**).

Expected for terminal bonded NCSe anions $\sim 2050 \text{ cm}^{-1}$.¹

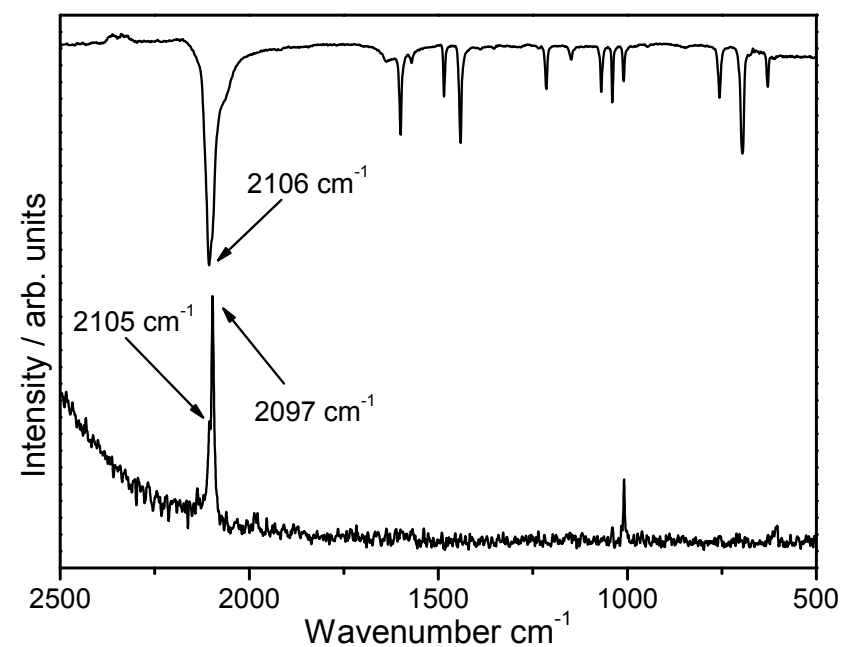


Figure S7. IR (top) and Raman (bottom) spectra for compound $[\text{Co}(\text{NCSe})_2(\text{pyridine})_2]_n$ (**2**).

Expected for μ -1,3 bridging NCSe anions $\geq 2100 \text{ cm}^{-1}$.¹

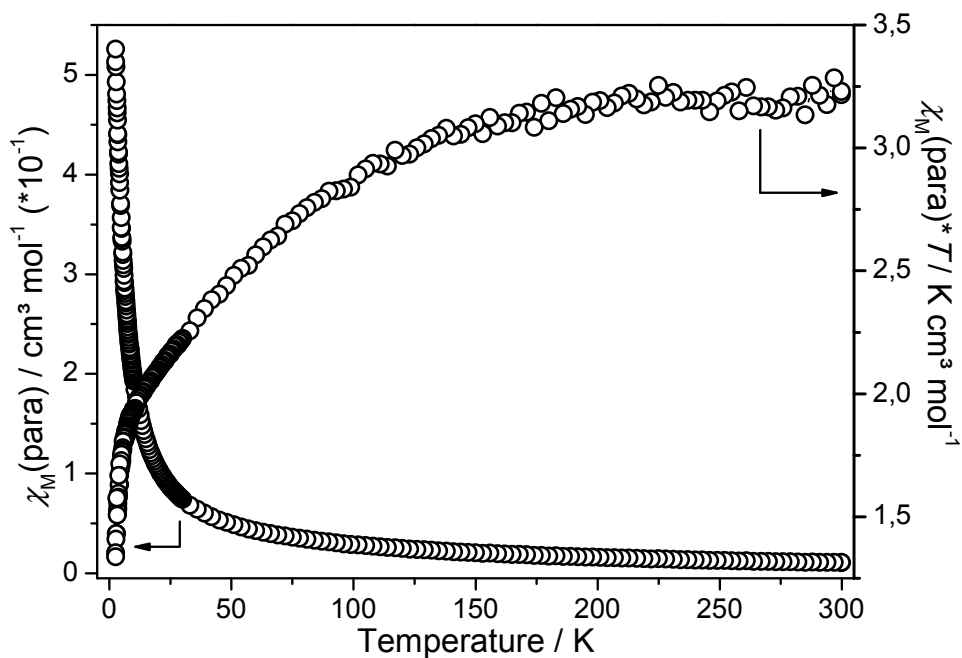


Figure S8. DC susceptibility measurements for $[\text{Co}(\text{NCSe})_2(\text{pyridine})_4]$ (**1**). The decrease of the $\chi_M^* T$ vs. T values are typical for Co^{II} cations and can be traced back to spin orbit coupling and zero field splitting.

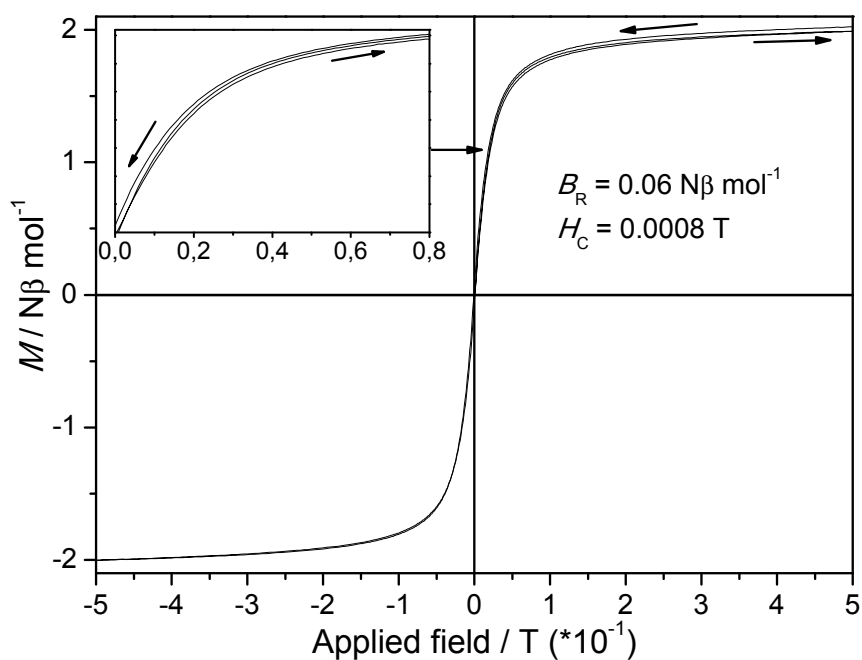


Figure S9. Magnetization saturation experiments for $[\text{Co}(\text{NCSe})_2(\text{pyridine})_2]_n$ (**2**). Hysteresis loop in the range of $\pm 0.5 \text{ T}$ and 4.5 K .

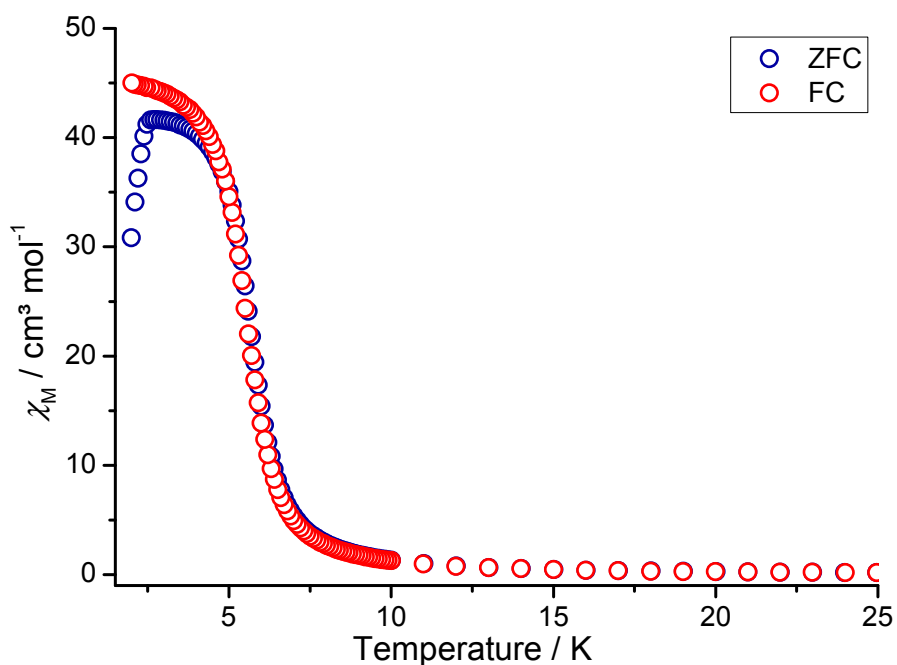


Figure S10. Zero-field-cooled (ZFC) and field-cooled (FC) magnetic susceptibility measurements at $H_{\text{DC}} = 0.01$ T.

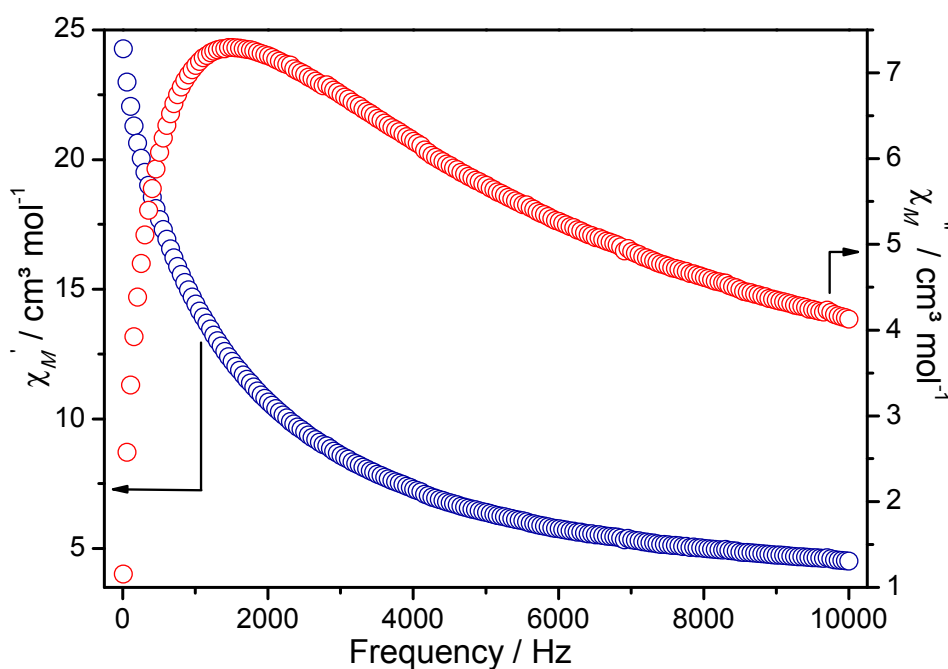


Figure S11. Isothermal frequency dependence of χ_M' and χ_M'' at 4.5 K for compound 2.

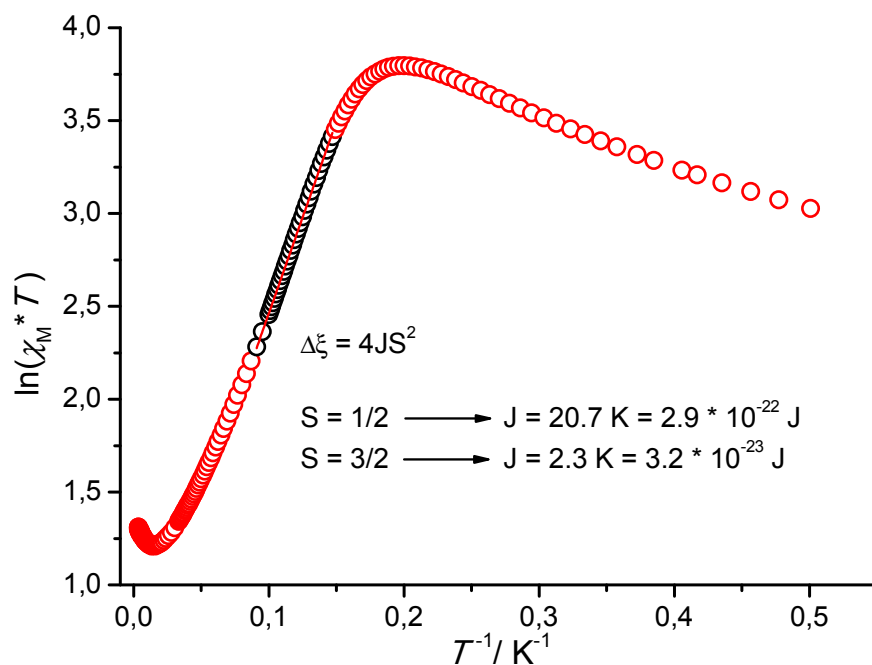


Figure S12. Plot of $\ln(\chi_M^* T)$ vs. T^{-1} for **2**.

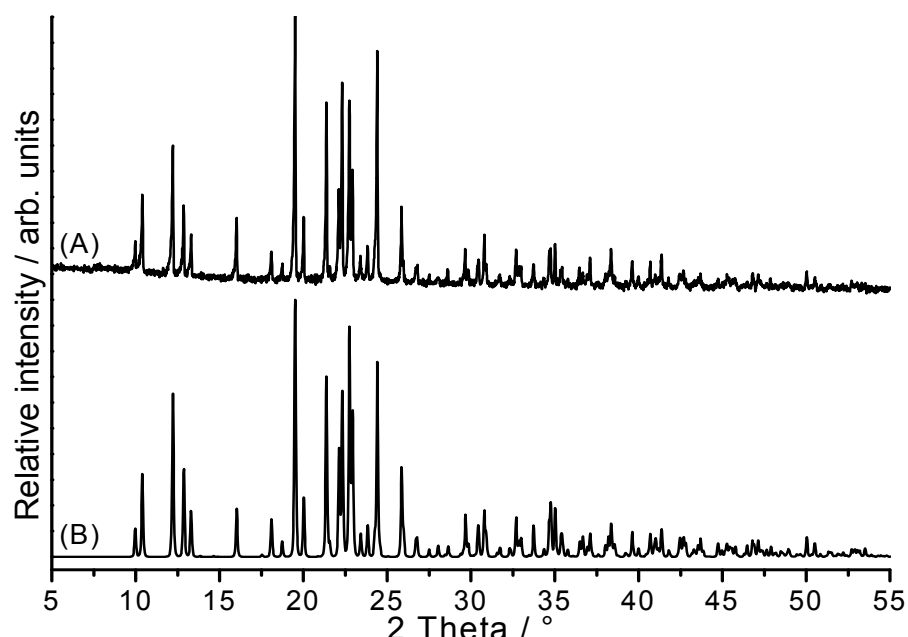


Figure S13. Experimental (A) and calculated (B) XRPD pattern for compound $[\text{Co}(\text{NCSe})_2(\text{pyridine})_4]$ (**1**).

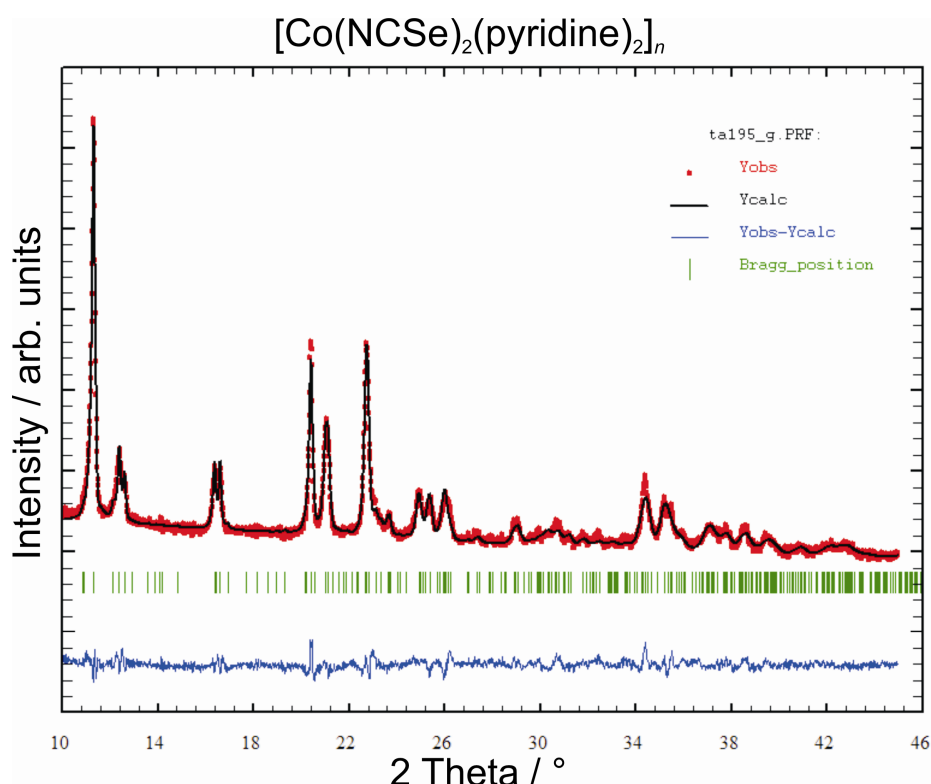


Figure S14. Difference plot of the Rietveld refinement of $[\text{Co}(\text{NCSe})_2(\text{pyridine})_4]$ (**1**).

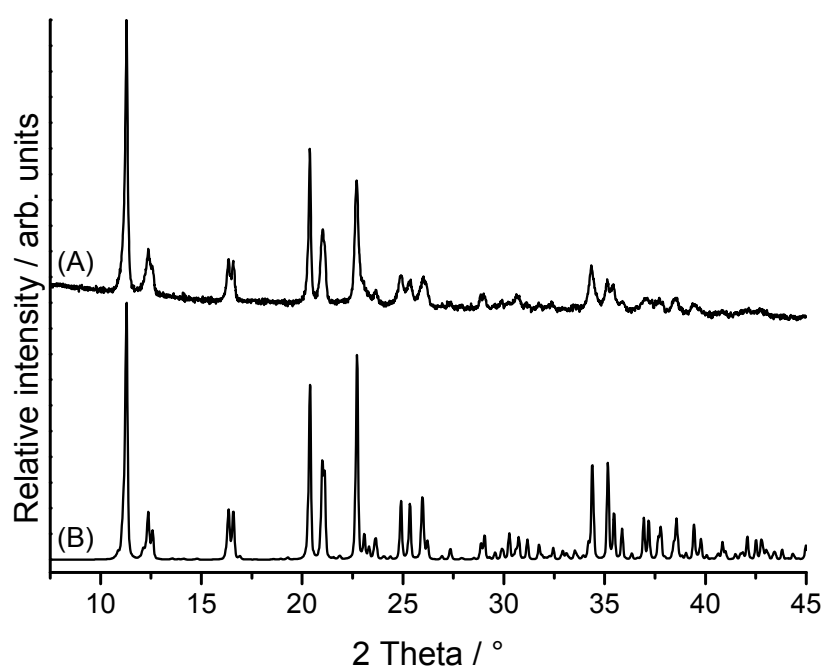


Figure S15. Experimental (A) and calculated (B) XRPD pattern for compound $[\text{Co}(\text{NCSe})_2(\text{pyridine})_2]_n$ (**2**).

Further experimental details

Rietveld Refinement. The Rietveld refinement was performed using *Fullprof2k* with the *Winplotr* software package.^{2, 3} The cell parameters were refined with *WinXPOW* Software package.⁴ After the initial refinements of the scale factors, unit cell parameters, and profile parameters, the organic part was refined using soft constrains for the pyridine and selenocyanato ligands. All atoms were refined isotropically and the H atoms were not considered.

Single-Crystal Structure Analysis. The investigation was performed with an imaging plate diffraction system (IPDS-2) with Mo-K α -radiation from STOE & CIE. The structure solution was done with direct methods using SHELXS-97⁵ and structure refinements were performed against $|F|^2$ using SHELXL-97.⁵ A numerical absorption correction was applied using X-Red Version 1.31 and X-Shape Version 2.11 of the Program Package X-Area.⁶ All non-hydrogen atoms were refined with anisotropic displacement parameters. All hydrogen atoms were positioned with idealized geometry and were refined with fixed isotropic displacement parameters [$U_{\text{eq}}(\text{H}) = -1.2 \cdot U_{\text{eq}}(\text{C})$] using a riding model with $d_{\text{C-H}} = 0.93 \text{ \AA}$.

X-ray Powder Diffraction (XRPD). XRPD experiments were performed using 1) a Stoe Transmission Powder Diffraction System (STADI P) with Cu-K α -radiation ($\lambda = 154.0598 \text{ pm}$) that is equipped with a linear position-sensitive detector (Delta 2 Theta = 6.5-7° simultaneous; scan range overall = 2-130°) from STOE & CIE and an Image Plate Detector (scan range overall = 0-127°) and 2) a PANalytical X'Pert Pro MPD Reflection Powder Diffraction System with Cu-K α radiation ($\lambda = 154.0598 \text{ pm}$) equipped with a PIXcel semiconductor detector from PANalytical.

Differential Thermal Analysis, Thermogravimetry, and Mass Spectroscopy (DTA-TG-MS).

The DTA-TG measurements were performed in a nitrogen atmosphere (purity: 5.0) in Al_2O_3 crucibles using a STA-409CD instrument from Netzsch. The DTA-TG-MS measurements were performed with the same instrument, which is connected to a quadrupole mass spectrometer from Balzers via Skimmer coupling from Netzsch. The MS measurements were performed in analogue and trend scan mode in Al_2O_3 crucibles in a dynamic nitrogen atmosphere (purity: 5.0) using heating rates of 4 °C/min. All measurements were performed with a flow rate of 75 mL/min. The instrument was calibrated using standard reference materials.

Spectroscopy. Fourier transform IR spectra were recorded on a Genesis series FTIR spectrometer, by ATI Mattson, in KBr pellets.

Magnetic measurements. Magnetic measurements were performed using a Physical Property Measuring System (PPMS) from Quantum Design, which is equipped with a 9 T magnet. The data were corrected for core diamagnetism.⁷

References

1. This reference refers to thiocyanato analogues, whose IR spectroscopic data should be similar with selenocyanates: R. A. Bailey, S. L. Kozak, T. W. Michelsen and W. N. Mills, *Coord. Chem. Rev.*, 1971, **6**, 407-445.
2. T. Roisnel and J. Rodriguez-Carvajal, Proceedings of the Seventh European Powder Diffraction Conference (EPDIC 7), 2000.
3. J. Rodriguez-Carvajal, *Physica B-Condensed Matter*, 1993, **192**, 55.
4. *WinXPOW, Version 2.23*, STOE & CIE GmbH, Darmstadt, Germany, 2003.
5. G. M. Sheldrick, *Acta Cryst.*, 2008, **A64**, 112-122.
6. *X-Area, Version 1.44, Program Package for Single Crystal Measurements*, STOE & CIE GmbH, Darmstadt, Germany, 2008.
7. G. A. Bain and J. F. Berry, *J. Chem. Educ.*, 2008, **85**, 532-536.